Microporous and Mesoporous Materials 151 (2012) 99–106

Contents lists available at SciVerse ScienceDirect

Microporous and Mesoporous Materials

journal homepage: www.elsevier.com/locate/micromeso

Phosphorus modified HMCM-22: Characterization and catalytic application in methanol-to-hydrocarbons conversion

Xin Wang [a], Weili Dai [a,b], Guangjun Wu [a], Landong Li [a,*], Naijia Guan [a], Michael Hunger [b,*]

[a] Key Laboratory of Advanced Energy Materials Chemistry (Ministry of Education), College of Chemistry, Nankai University, Tianjin 300071, PR China
[b] Institute of Chemical Technology, University of Stuttgart, 70550 Stuttgart, Germany

ARTICLE INFO

Article history:
Received 9 September 2011
Received in revised form 2 November 2011
Accepted 4 November 2011
Available online 13 November 2011

Keywords:
Phosphorus
HMCM-22
NMR
Methanol-to-hydrocarbons

ABSTRACT

In this work, a series of phosphorus-modified HMCM-22-*x*%P samples are prepared by impregnation of HMCM-22 with aqueous solution of $(NH_4)_2HPO_4$ and subsequent calcination. The phosphorus-modified HMCM-22 samples were characterized by means of XRD, NH_3-TPD, and multinuclear (^{31}P, ^{29}Si, ^{27}Al and ^{1}H) MAS NMR techniques. The phosphorus-modified HMCM-22 samples, together with parent HMCM-22, are studied as possible catalysts for methanol-to-hydrocarbons (MTH) reaction. HMCM-22-3%P exhibits very good MTH performance and 100% methanol conversion with *ca.* 70% selectivity to light olefins can be achieved within time-on-stream of 40 h at 723 K. The MTH reaction over H-MCM-22 and phosphorus-modified HMCM-22 is monitored by in situ UV/Vis spectra, and the hydrocarbon pool species occluded in spent catalysts are analyzed by ex situ GC–MS spectra. Based on the characterization and catalytic results, the modification effects of phosphorus on HMCM-22 and corresponding impacts on the MTH reaction are discussed.

1. Introduction

As an oil-free process to obtain hydrocarbons, the methanol-to-hydrocarbons (MTH) conversion on microporous solid acid catalysts has attracted extensive attentions since it was disclosed in 1970s [1]. During the past decades, a variety of molecular sieves have been explored as possible MTH catalysts [2–11] and it is generally acknowledged that the MTH performances of molecular sieves are controlled both by their framework structure and their acidity [12]. The silicoaluminophosphate-type zeolite HSAPO-34 and the aluminosilicate-type zeolite HZSM-5 are the most widely studied and promising catalysts for the MTH reaction. HSAPO-34, with moderate Brønsted acid sites and a well-defined pore structure of small entrances to large cages, can give a maximum light olefin yield of over 80% in the MTH reaction. Meanwhile, it has been commercialized in the more specialized methanol-to-olefins (MTO) process [13,14]. HZSM-5, with strong Brønsted acid sites and medium channel dimensions, is the catalyst initially studied for the MTH reaction [1], and nowadays HZSM-5 still attracts significant attentions due to its good resistance to deactivation by coke as well as its model behavior in MTH mechanism study [15–20].

The aluminosilicate-type zeolite MCM-22 (IZA code: MWW) contains two non-intersecting pore systems, both accessible through 10-membered ring only. One pore system is formed by two-dimensional sinusoidal 10-ring channels with an elliptical ring cross section of 0.41 nm × 0.51 nm. The other is formed by large cylindrical supercages of 0.71 nm in diameter (12-membered oxygen ring) and 1.82 nm in height [21]. Due to its peculiar framework structure, MCM-22 has been studied as possible catalyst for a series of reactions, e.g. isomerization [22,23], disproportionation [24], etherification [25], and alkylation [26] reactions. Recently, HMCM-22 has been applied in the MTH reaction and the attractive catalytic performances have been disclosed [27–29]. Since the acidity plays a key role in the MTH reaction, it is instructive to modify the acidity of MCM-22 to achieve better catalytic performances. Phosphorus modification is known as a feasible means to adjust the activity of aluminosilicate molecular sieves [30–32]. Particularly, phosphorus modification has been proven to be effective to change the product selectivity and to enhance the lifetime of HZSM-5 in MTH reaction [33–35].

In the present work, a series of phosphorus modified HMCM-22 samples were prepared by $(NH_4)_2HPO_4$ impregnation and characterized by means of XRD, NH_3-TPD, and solid-state NMR. The phosphorus modified HMCM-22 samples were studied as catalysts for the MTH reaction and the organic intermediates formed during reaction were analyzed by in situ UV/Vis spectra as well as ex situ GC–MS. Special emphasis was laid on the changes in the acidity

* Corresponding authors. Fax: +86 22 2350 0341 (L. Li), +49 711 685 64081 (M. Hunger).
E-mail addresses: lild@nankai.edu.cn (L. Li), michael.hunger@itc.uni-stuttgart.de (M. Hunger).

1387-1811/$ - see front matter © 2011 Elsevier Inc. All rights reserved.
doi:10.1016/j.micromeso.2011.11.008

and structure of HMCM-22 after phosphorus impregnation and the corresponding effects on MTH conversion.

2. Experimental

2.1. Sample preparation

Zeolite MCM-22 with the n_{Si}/n_{Al} ratio of 15 was synthesized using hexamethyleneimine as organic structure-directing agent according to the procedures described elsewhere [36]. The crystallized NaMCM-22 was converted to its proton form HMCM-22 by refluxing three times in 0.1 M NH_4NO_3 solution for 6 h, followed by drying at 343 K for 12 h and calcination at 873 K for 4 h. The P-modified HMCM-22 samples with P loadings of 1–4% were prepared by pore volume impregnation of HMCM-22 with desired amount of 0.5 M $(NH_4)_2HPO_4$ aqueous solution. The final product was dried at 343 K overnight, calcined at 873 K for 4 h in flowing synthetic air and labeled as HMCM-22-*x*%P, where *x* indicated the desired P loading.

2.2. Samples characterization

X-ray diffraction (XRD) patterns of the samples were recorded on a Bruker D8 diffractometer with Cu Kα radiation (λ = 1.5418 Å) from 5° to 50° with a scan speed of 2θ = 6.0°/min.

The surface areas and micropore volumes of the samples were measured by means of nitrogen adsorption performed at 77 K on a Quantachrome Autosorb 3B instrument. Prior to nitrogen adsorption, the samples were dehydrated at 473 K for 2 h.

The temperature-programmed desorption of ammonia (NH_3-TPD) was carried out in a quartz U-shaped reactor and was monitored by on-line chemisorption analyzer (Quantachrome ChemBet 3000). Sample of *ca*. 0.1 g was pretreated at 873 K for 1 h in He flow (30 ml/min), cooled to 373 K and saturated with 5% NH_3/He. After that, the sample was purged with He for 30 min to eliminate the physical absorbed ammonia. NH_3-TPD was then carried out in the range of 373–873 K at a heating rate of 10 K/min.

A HITACHI S-4700 Scanning Electron Microscope (SEM) was used for studying the morphology of HMCM-22 and SEM image was recorded on the sample covered with a thin layer of gold deposited by sputtering.

NMR experiments were performed on a Bruker Avance III spectrometer at resonance frequencies of 400.1, 104.3, 79.5, and 161.9 MHz for ^{1}H, ^{27}Al, ^{29}Si, and ^{31}P, respectively. The experimental conditions are as follows: single pulse excitation of $\pi/2$ for ^{1}H and ^{31}P, $\pi/6$ for ^{27}Al, and $\pi/4$ for ^{29}Si, and repetition times of 20 s for ^{1}H and ^{29}Si, 0.5 s for ^{27}Al, and 30 s for ^{31}P MAS NMR spectroscopy. The ^{1}H, ^{27}Al, and ^{31}P MAS NMR spectra were recorded with a sample spinning rate of 8 kHz, while the ^{29}Si MAS NMR spectra were obtained with 4 kHz. The ^{27}Al, ^{29}Si, and ^{31}P MAS NMR measurements were performed with hydrated samples. To avoid damage of the framework, the samples were exposed to an atmosphere that was saturated with vapor of a $Ca(NO_3)_2$ solution at ambient temperature to be fully hydrated 1 day before the NMR investigations. Before the ^{1}H MAS NMR experiments, the samples are dehydrated at 723 K at a pressure below 10^{-2} Pa for 12 h. After dehydration, the samples were sealed and kept in glass tubes until they were filled into the MAS NMR rotors in a glove box purged with dry nitrogen gas. Quantitative ^{1}H MAS NMR measurements were performed by a comparison of the signal intensities with that of an external intensity standard. The external standard consisted of dehydrated zeolite H,Na-Y (ion exchange degree of 35%) with 1.776 mmol protons/g and a weight of 58.5 mg. The decomposition and simulation of NMR spectra were carried out using the Bruker software WINNMR and WINFIT.

2.3. MTH reaction

The MTH reaction was performed in a fixed-bed reactor at atmospheric pressure. Typically, 0.4 g sample (sieve fraction, 0.25–0.5 mm) was placed in a stainless steel reactor (5 mm i.d.) and activated under flowing N_2 at 723 K for 0.5 h. Methanol was pumped in at 0.5 ml/h, corresponding to the weight hourly space velocity of 1/h. The products were analyzed on-line by gas chromatography equipped with a flame ionization detector and a packed-column Porapak Q to separate the C_1–C_8 hydrocarbons. The temperature of the column was maintained at 313 K for 15 min and then increased to 473 K at a rate of 10 K/min.

2.4. In situ UV/Vis studies of MTH reaction

The composition of the hydrocarbon pool compounds formed under reaction conditions was studied by in situ UV/Vis spectroscopy using a fiber-optic UV/Vis spectrometer [37]. Reference UV/Vis spectra of HMCM-22 and P modified samples were recorded at reaction temperature prior to the introduction of the methanol flow. UV/Vis spectra were conducted at 200–600 nm in the diffuse reflection mode with an AvaSpec-2048 Fiber Optic spectrometer, an AvaLight-DH-S deuterium light source by Avantes, and a glass fiber reflection probe HPSUV1000A by Oxford Electronics.

2.5. Characterization of occluded hydrocarbon pool species

The constitution of occluded hydrocarbon pool species in catalyst sample after the MTH reaction was analyzed by GC–MS. Typically, 0.3 g catalyst sample after reaction was carefully dissolved in 1 M HF solution. The solution was treated with CH_2Cl_2 to extract the organic compounds and the residual water was removed by the addition of sufficient sodium sulfate solid. Then, 1.0 μl CH_2Cl_2 organic extract was analyzed by GC–MS (Agilent 7890A/5975 MSD) with a DB-5 MS column (30 m, 0.25 mm i.d., stationary phase thickness 0.25 μm). The following temperature program was employed: isothermal at 313 K for 6 min, heating to 553 K with a rate of 10 K/min, and isothermal at 553 K for 10 min.

3. Results and discussion

3.1. Effect of phosphorus on the structure and acidity of HMCM-22

The XRD patterns of parent and phosphorus modified HMCM-22 samples are shown in Fig. 1. For HMCM-22, typical diffraction lines corresponding to the MWW structure are observed indicating that pure phase of the topology is obtained [38]. Phosphorus modified HMCM-22 samples exhibit identical diffraction patterns as that observed for parent HMCM-22, suggesting that the MWW structure is well preserved after the introduction of phosphorus.

The morphology of HMCM-22 was investigated by SEM and the corresponding image is shown in Fig. 2. Complex morphology is observed for HMCM-22, and disc-like platelets are prominent. Most of the platelets appear to be more than 5 μm in size, similar to previous report [28].

The acidic properties of parent and phosphorus modified HMCM-22 were evaluated by NH_3-TPD. The ammonia desorption profiles are shown in Fig. 3, and the quantitative analysis of NH_3-TPD results is summarized in Table 1. For all the samples, three types of ammonia desorption peaks can be observed: the low-temperature peaks at around 450 K and 525 K corresponding to weak acid sites and high-temperature peaks at around 700 K corresponding to strong acid sites. The amount of strong acid sites decreases distinctly with the increasing phosphorus loading from 0% to 4%, indicating that impregnation of phosphorus can mask

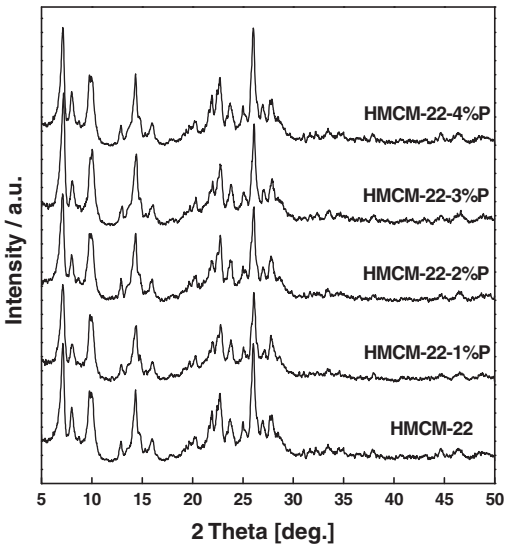

Fig. 1. XRD patterns of the parent and phosphorus modified HMCM-22 zeolites.

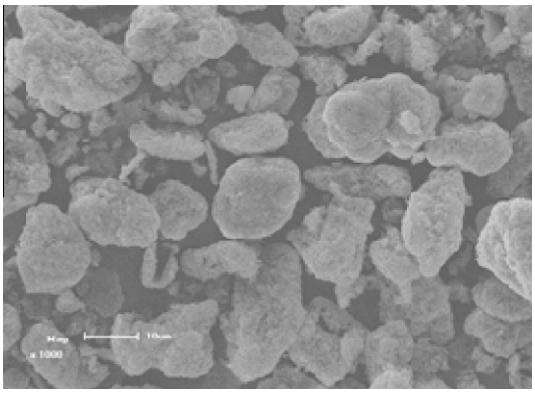

Fig. 2. SEM image of parent HMCM-22 zeolite.

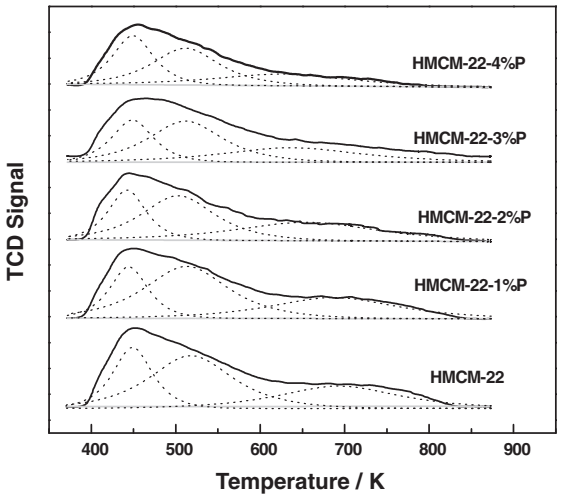

Fig. 3. NH_3-TPD profiles of the parent and phosphorus modified HMCM-22 zeolites.

the strong acid sites in HMCM-22. The amount of weak acid sites at $T = 525$ K also decreases with increasing phosphorus loading due to the mask of weak sites by phosphorus. In contrast, the amount of weak acid sites at $T = 450$ K first decreases with increasing phosphorus loading from 0% to 2%, and then increases with increasing with phosphorus loading from 2% to 4%. It is easily imagined that phosphorus impregnation may cause framework dealumination to some extent and thus produce some new weak acid sites, e.g. extra-framework AlOH species [32].

Table 1
Quantitative analysis of NH_3-TPD profiles of parent and phosphorus modified HMCM-22 samples.

Samples	Total amount (mmol/g)	Distribution of acid sites (mmol/g)		
		Strong acid ($T = 700$ K)	Weak acid I ($T = 525$ K)	Weak acid II ($T = 450$ K)
HMCM-22	1.34	0.35	0.62	0.37
HMCM-22-1%P	1.20	0.31	0.54	0.35
HMCM-22-2%P	1.08	0.28	0.49	0.31
HMCM-22-3%P	1.00	0.24	0.44	0.32
HMCM-22-4%P	0.92	0.19	0.38	0.35

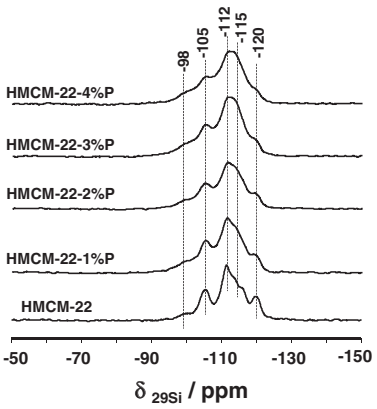

Fig. 4. ^{29}Si MAS NMR spectra of the parent and phosphorus modified HMCM-22 zeolites.

For a better understanding of phosphorus modification effects, multinuclear solid-state NMR technique was employed to analyze the changes in the local structure of HMCM-22 caused by phosphorus impregnation.

Fig. 4 shows the ^{29}Si MAS NMR spectra of the parent and phosphorus modified HMCM-22 samples. Due the different non-equivalent crystallographic T positions of the MWW structure of MCM-22, the ^{29}Si MAS NMR spectra of highly siliceous materials consist of Si(0Al) signals at −119.9, −115.8, −113.7, −112.4, −111.5, −110.8, and −105.5 ppm [39]. Some of these signals are caused by an overlap of the Si(0Al) signals of silicon atoms at different crystallographic positions. In the presence of Si(1Al) species, additional signals at −112.5, −110.5, −107.5, −104.5, and −98.0 ppm may occur [40]. Furthermore, it is generally accepted that Q^3 silicon species (Si(3Si,1OH) at defect sites in zeolites and amorphous aluminosilicates cause signals at −103 ppm (see e.g. Ref. [41]). For the ^{29}Si MAS NMR spectra shown in Fig. 3, a significant broadening of all signals with increasing phosphorus modification occurs. This indicates an attack of phosphorus atoms to the silicon atoms at all crystallographic positions. Furthermore, a decrease of the signal at −105 ppm could be a hint to a decrease of SiOH groups at −103 ppm, which was studied in detail by ^{1}H MAS NMR spectroscopy (vide supra).

Fig. 5 shows the ^{27}Al MAS NMR spectra of the parent and phosphorus modified HMCM-22 samples. Strong signals at 48–60 ppm

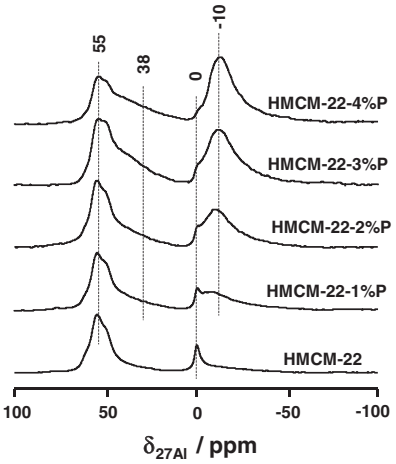

Fig. 5. ^{27}Al MAS NMR spectra of the parent and phosphorus modified HMCM-22 zeolites.

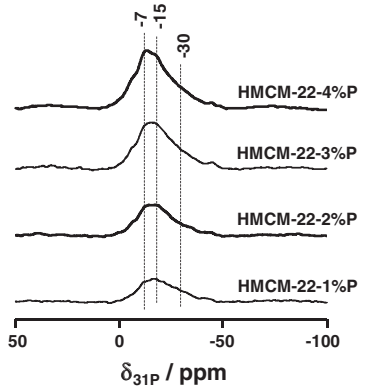

Fig. 6. ^{31}P MAS NMR spectra of phosphorus modified HMCM-22 zeolites.

are observed for all samples and these signals should be attributed to tetrahedrally coordinated aluminum at different non-equivalent framework positions [40,42]. The weak signal at 0 ppm indicates the presence of octahedrally coordinated aluminum species probably due to a small quantity of extra-framework aluminum atoms [40,42]. With the introduction of phosphorus to the parent HMCM-22 material, two new signals, i.e. a broad hump at 38 and a strongly increasing signal at −10 ppm, appear. The broad signal centered at 38 ppm is attributed to tetrahedral aluminum in distorted environment at either framework [43] or non-framework positions [44], and the signal at −10 ppm is attributed to octahedral aluminum atoms attached to phosphorus atoms [32]. With increasing phosphorus loading, the intensities of the signals at 38 and −10 increase, while the intensity of signal at 55 ppm decreases slightly. These observations strongly indicate that dealumination process occurs induced by the phosphorus impregnation.

The chemical states of phosphorus in HMCM-22 are investigated by ^{31}P MAS NMR spectroscopy (Fig. 6). The broad signals occurring in the ^{31}P MAS NMR spectra reveal the interaction of phosphorus with the HMCM-22 framework and the presence of phosphorus in different environments. Typically, the signal at −7 ppm is due to the terminal phosphorus atoms in $H_4P_2O_7$ species and the signal at −15 ppm is due to the middle phosphorus atoms in polyphosphate or polymerized short-chain polyphosphates [45,46]. The broad signals at −20 to −40 ppm are mainly due to extra-framework aluminum phosphate and condensed polyphosphate [47]. The intensities of all these signals increase with increasing phosphorus loading. The results from ^{31}P MAS NMR spectra indicate that phosphorus species exist mainly in the form of polyphosphates on the modified HMCM-22 zeolites.

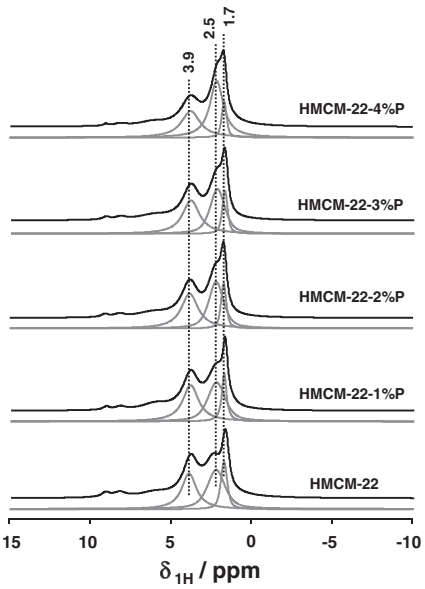

Fig. 7. ^{1}H MAS NMR spectra of the parent and phosphorus modified HMCM-22 zeolites.

Table 2
Hydroxyl coverage and textual properties of the parent and phosphorus modified HMCM-22 samples.

Sample	OH concentration (mmol/g)[a]			n_{Si}/n_{Al}[b]	P loading (%)[b]	Micropore volume (ml/g)[c]	Surface area (m^2/g)
	n_{SiOH}	n_{AlOH}	n_{SiOHAl}				
HMCM-22	0.15	0.27	0.31	15.3	–	0.20	469
HMCM-22-1%P	0.12	0.29	0.30	15.7	0.9	0.20	447
HMCM-22-2%P	0.11	0.30	0.26	16.1	1.9	0.20	445
HMCM-22-3%P	0.10	0.32	0.23	15.9	2.8	0.19	438
HMCM-22-4%P	0.07	0.41	0.18	16.2	3.7	0.19	429

[a] Determined by ^{1}H MAS NMR.
[b] Determined by ICP-AES.
[c] Determined by nitrogen adsorption.

The hydroxyl groups in the parent and phosphorus modified HMCM-22 samples were studied by means of ^{1}H MAS NMR spectra, as shown in Fig. 7. The signal at 1.7 ppm is ascribed to silanol groups at framework defects, while the signal at 2.5 ppm is due to hydroxyl groups bonded to extra-framework aluminum species [48]. Most interestingly, the signal at 3.9 ppm indicates the presence of acidic bridging hydroxyl groups (SiOHAl), i.e. the Brønsted acid sites of HMCM-22 [49]. The quantitative analysis of the hydroxyl signal of the samples after phosphorus impregnation is summarized in Table 2. It is seen that the introduction of phosphorus results in significant decrease in Brønsted acid site density of HMCM-22. Typically, the concentration of Brønsted acid sites decreased from 0.31 mmol/g in the parent HMCM-22 zeolite to 0.18 mmol/g in HMCM-22-4%P. Simultaneously, the concentration of silanol groups at framework defects decreased, while the concentration of hydroxyl groups bonded to extra-framework aluminum species increased upon phosphorus impregnation.

Considering the results of ^{1}H, ^{27}Al, ^{29}Si and ^{31}P MAS NMR spectroscopy, we conclude that phosphorus impregnation shows great

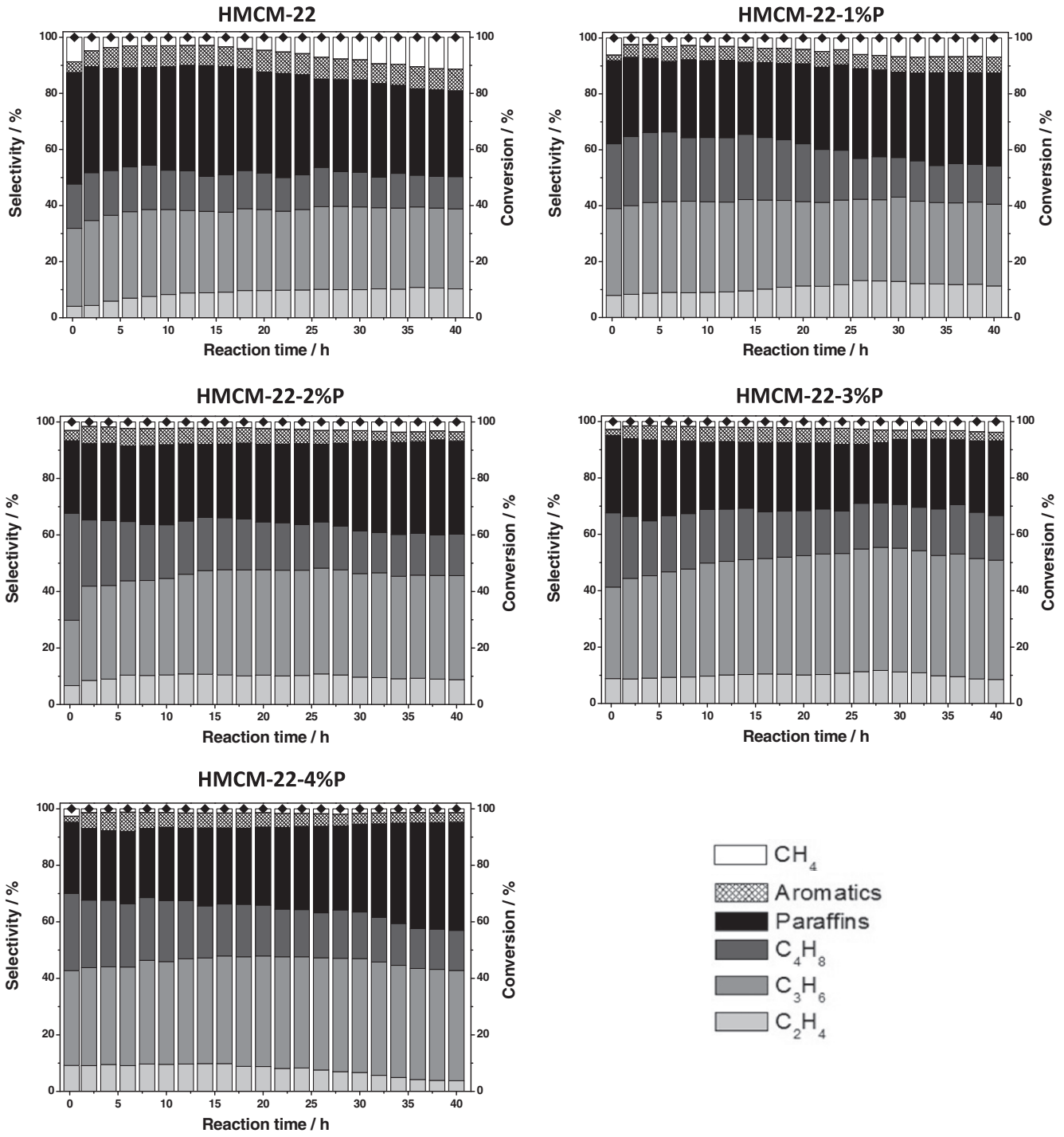

Fig. 8. Methanol conversion and product selectivity during the MTH conversion on the parent and phosphorus modified HMCM-22 zeolites at 723 K.

modification effects on both the acidity and structure of the parent HMCM-22 zeolite. The phosphorus species, with in final form of polyphosphates, prefer to react with framework aluminum species and lead to the partial breakage of Si–O–Al bonds, displayed as dealumination of the zeolite framework and a decrease of Brønsted acid site density.

3.2. Effect of phosphorus on the MTH performances

Fig. 8 shows the methanol conversion and product selectivity during the MTH conversion on parent and phosphorus modified HMCM-22 at 723 K. A complete conversion of methanol is observed for all samples and no deactivation occurs within time-on-stream (TOS) of 40 h, which can be ascribed to the good diffusion properties of the product molecules in the MWW channels. For the parent HMCM-22 zeolite, the selectivity to light olefins (C_2–C_4) is stable and kept at *ca.* 50% within 40 h. In this period, a large quantity of paraffins (*ca.* 40%) and a small quantity of aromatics (<10%) could be detected in the product. The product selectivity in MTH reaction over HMCM-22 is similar to that reported by Min et al. [27] using HMCM-22 (Si/Al = 16.8) as catalysts. While the methanol conversion in this work is much more stable, which

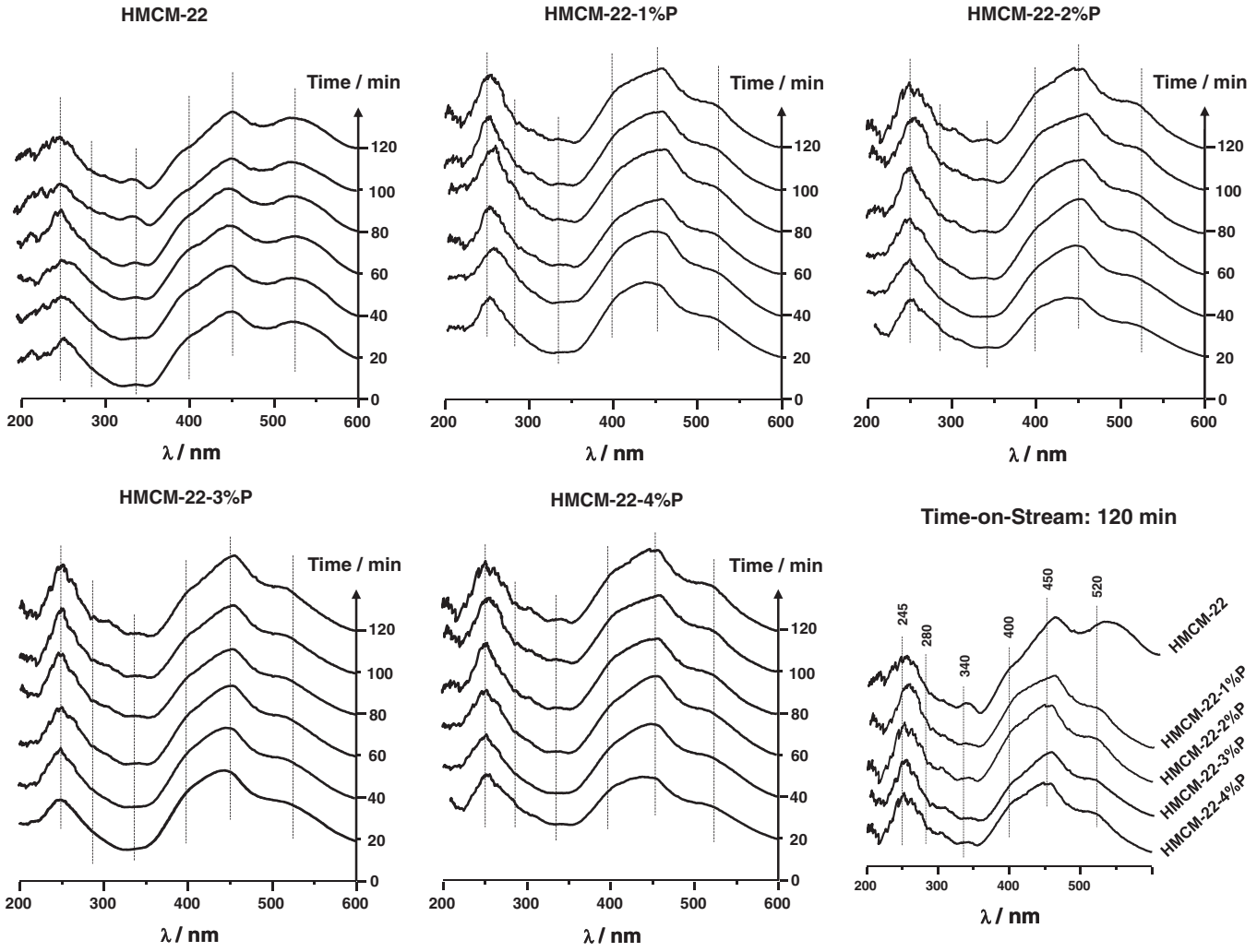

Fig. 9. In situ UV/Vis spectra recorded during MTH reaction on the parent and phosphorus modified HMCM-22 zeolites at 723 K.

might be explained by the different reaction conditions and feed composition employed. The introduction of phosphorus to HMCM-22 significantly changes the product distribution of the MTH reaction. The formation of paraffins and aromatics is suppressed to some extent, while the production of light olefins, especial propylene, is enhanced. The phosphorus loading on HMCM-22 also shows distinct effects on the product selectivity. The highest selectivity to light olefins of *ca*. 70% could be achieved on HMCM-22-3%P. Considering the fact that the light olefins are the more desirable products from MTH process, HMCM-22-3%P is the most promising MTH catalyst for potential applications.

3.3. In situ UV/Vis results

The in situ UV/Vis spectra recorded during MTH reaction on parent and phosphorus modified HMCM-22 at 723 K are shown in Fig. 9. Comparing the different catalysts under study, similar organic species were formed during the MTH reaction as indicated by UV/Vis bands at 245, 280, 340, 400, 450, and 520 nm. The band at 245 nm hints to the formation of dienes [37], while bands at 340, 450 and 520 nm are due to dienylic carbenium ions, trienylic carbenium ions, and poly-enylic carbenium ions, respectively [50,51]. Furthermore, the bands at 280 and 400 nm indicate the formation of polyalkylaromatics and polycyclic aromatics, respectively [10,37]. Polyalkylaromatics and dienylic carbenium ions are active hydrocarbon pool species in the olefin production, while poly-enylic carbenium ions and polycyclic aromatics may be responsible for coke formation and the catalyst deactivation [12]. From the time-resolved UV/Vis spectra, the slow accumulation of organic species is observed within time-on-stream of 1 h. After TOS = 1 h, the concentration of all organic species, reflected by the intensities of corresponding UV/Vis bands, remain almost unchanged. This may be the reason for the stable MTH activity of all HMCM-22 zeolites under study for a time-on-stream of 40 h. For comparison, the UV/Vis spectra of the different HMCM-22 samples recorded at reaction times up to TOS = 2 h are shown in Fig. 9. According to these spectra, the phosphorus impregnation significantly decreases the amount of enylic carbenium ions as indicated by the UV/Vis bands at 340, 450, and 520 nm. Considering that carbenium ions are formed on the Brønsted acid sites [52], the decrease of Brønsted acid sites in HMCM-22 by phosphorus impregnation undoubtedly leads to a smaller number of carbenium ions formed. Moreover, the decrease of trienylic carbenium ions and poly-enylic carbenium ions is observed to be more pronounced than the decrease of dienylic carbenium ions.

3.4. GC–MS analysis of occluded hydrocarbon pool species

The exact constitution of the occluded hydrocarbon pool compounds in the spent catalyst samples is analyzed by ex situ GC–

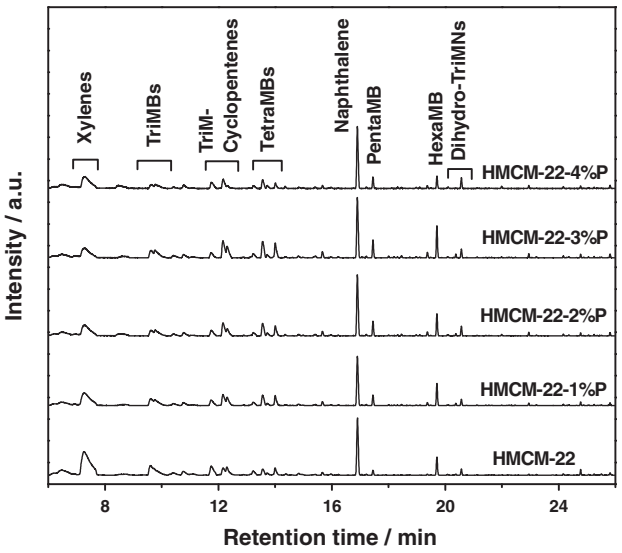

Fig. 10. GC–MS analysis of occluded hydrocarbon pool species in the parent and phosphorus modified HMCM-22 zeolites after MTH reaction at 723 K for 40 h.

MS and the results are shown in Fig. 10. The selected peak assignments are made by comparing their mass spectra with the NIST database [53]. It is known that the constitution of hydrocarbon pool species occluded in the zeolites is strongly dependent on the topology [54]. Since the MWW structure of MCM-22 is well preserved after phosphorus impregnation, similar types of organic species are detected in the parent and phosphorus modified HMCM-22. Typically, methylbenzenes, naphthalene and methylnaphthalenes were observed as major hydrocarbon pool species occluded in samples after MTH reaction for 40 h, similar to literature reports [27,28]. Furthermore, the introduction of phosphorus to HMCM-22 changes the relative intensity of different hydrocarbon pool species. For example, the relative intensity of higher methylbenzenes (tetra-methylbenzenes, penta-methylbenzenes, and hexa-methylbenzenes) increases with increasing phosphorus loading, reaches to a maximum at phosphorus loading of *ca.* 3%, and then decreases with further increasing phosphorus loading. The number of methyl groups in methyl-substituted benzene rings is reported to regulate the type of light olefins formed. In this connection, propylene formation is highly favored by higher methylbenzenes as hydrocarbon pool species [16,55]. In the present study, the highest selectivity to propylene is obtained on HMCM-22-3%P with the highest relative intensity of higher methylbenzenes.

4. Conclusion

Phosphorus modified HMCM-22 zeolites with phosphorus loadings of 0–4% have been prepared by impregnation of parent HMCM-22 (n_{Si}/n_{Al} = 15) with $(NH_4)_2HPO_4$ and subsequent calcination. The as-prepared phosphorus modified HMCM-22 samples were characterized by means of XRD, NH_3-TPD, and multinuclear MAS NMR techniques. According to the characterization results, the MWW framework structure of HMCM-22 was well preserved after the introduction of phosphorus, while the textual properties of the parent HMCM-22 material were adjusted. Most importantly, the amount of Brønsted acid sites in HMCM-22 was strongly decreased by phosphorus impregnation. The parent and phosphorus-modified HMCM-22 zeolites were tested as possible catalysts for the MTH reaction, and a 100% methanol conversion could be obtained for all catalyst samples and preserved for 40 h at 723 K. The introduction of phosphorus to HMCM-22 could efficiently change the product distribution during the MTH reaction. Typically, *ca.* 70% selectivity to light olefins with *ca.* 40% selectivity to propylene could be achieved on HMCM-22-3%P. In situ UV/Vis spectra revealed that dienes, enylic carbenium, and aromatics are formed in HMCM-22 during MTH reaction, while the introduction of phosphorus to HMCM-22 can efficiently decrease the enylic carbenium ions formed. GC–MS analysis results indicated that the relative intensity of higher methylbenzenes, including tetra-methylbenzenes, penta-methylbenzenes, and hexa-methylbenzenes, can be improved by phosphorus impregnation, which is responsible for the enhanced selectivity to propylene.

Acknowledgements

This work is supported by the National Basic Research Program of China (2009CB623502) and MOE (IRT0927). Furthermore, M.H. wants to thank for financial support by Fonds der Chemischen Industrie and Deutsche Forschungsgemeinschaft.

References

[1] C.-D. Chang, Catal. Rev. Sci. Eng. 25 (1983) 1–118.
[2] M. Stöcker, Micropor. Mesopor. Mater. 29 (1999) 3–48.
[3] M.A. Djieugoue, A.M. Prakash, L. Kevan, J. Phys. Chem. B 104 (2000) 6452–6461.
[4] Z. Zhu, M. Hartmann, L. Kevan, Chem. Mater. 12 (2000) 2781–2787.
[5] A.T. Aguayo, A.G. Gayubo, R. Vivanco, M. Olazar, J. Bilbao, Appl. Catal. A 283 (2005) 197–207.
[6] A.G. Gayubo, A.T. Aguayo, A. Alonso, A. Atutxa, J. Bilbao, Catal. Today 106 (2005) 112–117.
[7] S. Svelle, U. Olsbye, F. Joensen, M. Bjørgen, J. Phys. Chem. C 111 (2007) 17981–17984;
M. Castro, S.J. Warrender, P.A. Wright, D.C. Apperley, Y. Belmabkhout, G. Pirngruber, H.K. Min, M.B. Park, S.B. Hong, J. Phys. Chem. C 113 (2009) 15731–15741.
[8] J.W. Park, S.J. Kim, M. Seo, S.Y. Kim, Y. Sugi, G. Seo, Appl. Catal. A 349 (2008) 76–85.
[9] J.H. Lee, M.B. Park, J.K. Lee, H.K. Min, M.K. Song, S.B. Hong, J. Am. Chem. Soc. 132 (2010) 12971–12982.
[10] W. Dai, X. Wang, G. Wu, N. Guan, M. Hunger, L. Li, ACS Catal. 1 (2011) 292–299.
[11] J. Li, Y. Wei, G. Liu, Y. Qi, P. Tian, B. Li, Y. He, Z. Liu, Catal. Today 117 (2011) 221–228.
[12] J.-F. Haw, W. Song, D.-M. Marcus, J.-B. Nicholas, Acc. Chem. Res. 36 (2003) 317–326.
[13] S. Wilson, P. Barger, Micropor. Mesopor. Mater. 29 (1999) 117–126.
[14] J.Q. Chen, A. Bozzano, B. Glover, T. Fuglerud, S. Kvisle, Catal. Today 106 (2005) 103–107.
[15] B. Valle, A. Alonso, A. Atutxa, A.G. Gayubo, J. Bilbao, Catal. Today 106 (2005) 118–122.
[16] M. Bjørgen, S. Svelle, F. Joensen, J. Nerlov, S. Kolboe, F. Bonino, L. Palumbo, S. Bordiga, U. Olsbye, J. Catal. 249 (2007) 195–207.
[17] L. Palumbo, F. Bonino, P. Beato, M. Bjørgen, A. Zecchina, S. Bordiga, J. Phys. Chem. C 112 (2008) 9710–9716.
[18] M. Bjørgen, F. Joensen, K.P. Lillerud, U. Olsbye, S. Svelle, Catal. Today 142 (2009) 90–97.
[19] J. Kim, M. Choi, R. Ryoo, J. Catal. 269 (2010) 219–228.
[20] H. Yamazaki, H. Shima, H. Imai, T. Yokoi, T. Tatsumi, J.N. Kondo, Angew. Chem., Int. Ed. 50 (2011) 1853–1856.
[21] M.E. Leonowicz, J.A. Lawton, S.L. Lawton, M.K. Rubin, Science 264 (1994) 1910–1913.
[22] Y. Shang, P.P. Yang, M.J. Jia, W.X. Zhang, T.H. Wu, Catal. Commun. 9 (2008) 907–912.
[23] A. Corma, C. Corell, F. Flopis, A. Martínez, J. Pérez-Pariente, Appl. Catal. A 115 (1994) 121–134.
[24] P. Wu, T. Komatsu, T. Yashima, Micropor. Mesopor. Mater. 22 (1998) 343–356.
[25] M.J. Verhoef, E.J. Creyghton, J.A. Peters, H. van Bekkum, Chem. Commun. (1997) 1989–1990.
[26] Z.R. Zhu, Q.L. Chen, W. Zhu, D.J. Kong, C. Li, Catal. Today 93–95 (2004) 321–325.
[27] H.K. Min, M.B. Park, S.B. Hong, J. Catal. 271 (2010) 186–194.
[28] M. Bjørgen, S. Akyalcin, U. Olsbye, S. Benard, S. Kolboe, S. Svelle, J. Catal. 275 (2010) 170–180.
[29] A. Lacarriere, F. Luck, D. Świerczyński, F. Fajula, V. Hulea, Appl. Catal. A 402 (2011) 208–217.
[30] H. Vinek, G. Rumplmayr, J.A. Lercher, J. Catal. 115 (1989) 291–300.
[31] G. Caeiro, P. Magnoux, J.M. Lopes, F. Ramôa Ribeiro, S.M.C. Menezes, A.F. Costa, H.S. Cerqueira, Appl. Catal. A 314 (2006) 160–171.

[32] G.L. Zhao, J.W. Teng, Z.K. Xie, W.Q. Jin, W.M. Yang, Q.L. Chen, Y. Tang, J. Catal. 248 (2007) 29–37.
[33] S.M. Abubakar, D.M. Marcus, J.C. Lee, J.O. Ehresmann, C.Y. Chen, P.W. Kletnieks, D.R. Guenther, M.J. Hayman, M. Pavlova, J.B. Nicholas, J.F. Haw, Langmuir 22 (2006) 4846–4852.
[34] M. Kaarsholm, F. Joensen, J. Nerlov, R. Cenni, J. Chaouki, G.S. Patience, Chem. Eng. Sci. 62 (2007) 5527–5532.
[35] J. Liu, C.X. Zhang, Z.H. Shen, W.M. Hua, Y. Tang, W. Shen, Y.H. Yue, H.L. Xu, Catal. Commun. 10 (2009) 1506–1509.
[36] A. Corma, C. Corell, J. Pérez-Pariente, Zeolites 15 (1995) 2–8.
[37] Y. Jiang, J. Huang, J. Weitkamp, M. Hunger, Stud. Surf. Sci. Catal. 170 (2007) 1137–1144.
[38] M.M.J. Treacy, J.B. Higgins, Higgins. Collection of Simulated XRD Powder Patterns for Zeolites, fifth revised ed., Elsevier, 2007.
[39] G.J. Kennedy, S.L. Lawton, M.K. Rubin, J. Am. Chem. Soc. 116 (1994) 11000–11003.
[40] M. Hunger, S. Ernst, J. Weitkamp, Zeolites 15 (1995) 188–192.
[41] J. Barras, J. Klinowski, J. Chem. Soc., Faraday Trans. 90 (1994) 3719–3723.
[42] C. Delitala, M.D. Alba, A.I. Becerro, D. Delpiano, D. Meloni, E. Musu, I. Ferino, Micropor. Mesopor. Mater. 118 (2009) 1–10.
[43] Z. Yan, D. Ma, J. Zhuang, X. Liu, X. Liu, X. Han, X. Bao, F. Chang, L. Xu, Z. Liu, J. Mol. Catal. A 194 (2003) 153–167.
[44] S.M.C. Menezes, V.L. Camorim, Y.L. Lam, R.A.S. San Gil, A. Bailly, J.P. Amoureux, Appl. Catal. A 207 (2001) 367–377.
[45] G. Seo, R. Ryoo, J. Catal. 124 (1990) 224–230.
[46] G. Lischke, R. Eckelt, H.G. Jerschkewitz, B. Parlitz, E. Schreier, W. Storek, B. Zibrowius, G. Ohlmann, J. Catal. 132 (1991) 229–243.
[47] J. Zhuang, D. Ma, G. Yang, Z. Yan, X. Liu, X. Liu, X. Han, X. Bao, P. Xie, Z. Liu, J. Catal. 228 (2004) 234–242.
[48] M. Hunger, S. Ernst, S. Steuernagel, J. Weitkamp, Micropor. Mater. 6 (1996) 349–353.
[49] M. Hunger, Catal. Rev. Sci. Eng. 39 (1997) 345–393.
[50] I. Kiricsi, H. Foerster, G. Tasi, J.B. Nagy, Chem. Rev. 99 (1999) 2085–2114.
[51] S. Yang, J.N. Kondo, K. Domen, Catal. Today 73 (2002) 113–125.
[52] W. Dai, M. Scheibe, N. Guan, L. Li, M. Hunger, ChemCatChem 3 (2011) 1130–1133.
[53] NIST Chemistry Web book, <http://www.webbook.nist.gov/chemistry>.
[54] J.W. Park, J.Y. Lee, K.S. Kim, S.B. Hong, G. Seo, Appl. Catal. A 339 (2008) 36–44.
[55] W. Song, H. Fu, J.F. Haw, J. Am. Chem. Soc. 123 (2001) 4749–4754.